CellPress

Structure
Article

Structural and Functional Characterization of the Phosphorylation-Dependent Interaction between PML and SUMO1

Laurent Cappadocia,[1,3,4] Xavier H. Mascle,[1,3,4] Véronique Bourdeau,[1] Samuel Tremblay-Belzile,[1] Malik Chaker-Margot,[1] Mathieu Lussier-Price,[1] Junya Wada,[2] Kazuyasu Sakaguchi,[2] Muriel Aubry,[1] Gerardo Ferbeyre,[1] and James G. Omichinski[1,*]

[1]Département de Biochimie et Médicine Moléculaire, Université de Montréal, C.P. 6128 Succursale Centre-Ville, Montréal, QC H3C 3J7, Canada

[2]Department of Chemistry, Faculty of Science, Hokkaido University, Sapporo 060-0810, Japan

[3]Co-first author

[4]Present address: Structural Biology Program, Sloan-Kettering Institute, New York, NY 10065, USA

*Correspondence: jg.omichinski@umontreal.ca

http://dx.doi.org/10.1016/j.str.2014.10.015

SUMMARY

PML and several other proteins localizing in PML-nuclear bodies (PML-NB) contain phosphoSIMs (SUMO-interacting motifs), and phosphorylation of this motif plays a key role in their interaction with SUMO family proteins. We examined the role that phosphorylation plays in the binding of the phospho-SIMs of PML and Daxx to SUMO1 at the atomic level. The crystal structures of SUMO1 bound to un-phosphorylated and tetraphosphorylated PML-SIM peptides indicate that three phosphoserines directly contact specific positively charged residues of SUMO1. Surprisingly, the crystal structure of SUMO1 bound to a diphosphorylated Daxx-SIM peptide indicate that the hydrophobic residues of the phosphoSIM bind in a manner similar to that seen with PML, but important differences are observed when comparing the phosphorylated residues. Together, the results provide an atomic level description of how specific acetylation patterns within different SUMO family proteins can work together with phosphorylation of phosphoSIM's regions of target proteins to regulate binding specificity.

INTRODUCTION

Like ubiquitin, SUMO proteins (SUMO 1–3) can be covalently attached to lysine residues in target proteins through a post-translational modification that involves three enzymatic reactions (Desterro et al., 1999; Kahyo et al., 2001; Pichler et al., 2002). One important feature that regulates the overall SUMOylation pathway is the existence of SUMO-binding domains (SBDs) that mediate noncovalent protein-protein interactions with either SUMO family proteins or proteins that have been SUMOylated. Although numerous ubiquitin-binding domains (UBDs) have been identified (Husnjak and Dikic, 2012), only two types of SBDs have been characterized to date; a SUMO-specific zinc-finger domain (ZZ-zinc finger) (Danielsen et al., 2012) and the more prevalent SUMO-interacting motif (SIM) (Song et al., 2004). The minimal core of the SIM is characterized by a short sequence composed predominantly of hydrophobic residues, ΨΨΨΨ, ΨxΨΨ, or ΨΨxΨ (where Ψ is V, I, or L and x is typically D, E, S, or T) (Gareau and Lima, 2010). Upon binding to SUMO proteins, the SIM forms either a parallel or an antiparallel β strand configuration with the second β strand of SUMO proteins, and the orientation of the SIM (parallel versus antiparallel) toward a specific SUMO protein is thought to be dictated by acidic and/or phosphorylated amino acid residues juxtaposed to the hydrophobic core of the SIM (Gareau and Lima, 2010; Gareau et al., 2012; Song et al., 2005).

The best-characterized interactions involving SIMs and either SUMO proteins or SUMOylated proteins occurs during promyelocytic leukemia (PML)-dependent recruitment of proteins into subnuclear structures known as PML-nuclear bodies (PML-NBs) (Cho et al., 2009; Ishov et al., 1999; Lin et al., 2006; Rasheed et al., 2002; Sung et al., 2011). PML is implicated in regulating a wide range of biological processes, including transcription, cell cycle control, and genome integrity (Dellaire and Bazett-Jones, 2007; Salomoni et al., 2012; Zhong et al., 2000). Due to alternative splicing, the *PML* gene gives rise to several protein isoforms (Jensen et al., 2001), and all nuclear PML isoforms, except PML-VI, have a SIM and are components of PML-NBs (Maroui et al., 2012; Weidtkamp-Peters et al., 2008). Although the function of the PML-NBs remains enigmatic, it is known that a wide variety of proteins transit in and out of PML-NBs dynamically in response to different stimuli, including oncogenic stress, radiation damage, cytokine signaling, and viral infection (Lallemand-Breitenbach and de Thé, 2010). Interestingly, PML plays a key role in regulating the transit of these proteins through noncovalent interactions between its SIM and SUMOylated proteins or by the fact that it is SUMOylated and interacts with other proteins that contain SIMs (Chen et al., 2008; Dellaire et al., 2006; Everett et al., 1999; Salomoni et al., 2005; Weidtkamp-Peters et al., 2008).

The SIM found in PML is composed of four hydrophobic residues (VVVI) followed by a cluster of serine and acidic residues (Shen et al., 2006; Song et al., 2004). Within the serine/acidic

residue-rich cluster, there are three consensus casein kinase 2 (CK2)-phosphorylation sites, and a fourth consensus CK2-phosphorylation site is generated subsequent to phosphorylation of the C-terminal site (Scaglioni et al., 2006; Rabellino et al., 2012). Initially, it was suggested that PML degradation rates are enhanced by phosphorylation of these serine residues based on the observation that blocking phosphorylation of these residues by mutating them to alanine significantly enhanced PML stability (Scaglioni et al., 2006). In addition, several tumor-derived cell lines displayed an inverse relationship between their CK2 activity and their levels of PML protein (Scaglioni et al., 2006, 2008; Rabellino et al., 2012). Of note, mutating the serines to alanines led to a decrease in PML binding to SUMO1 as well as an enhancement of PML-driven apoptosis (Percherancier et al., 2009; Scaglioni et al., 2006; Stehmeier and Muller, 2009). These results suggest that several PML functions can be regulated by varying the phosphorylation status of the serine residues adjacent to the hydrophobic core of the SIM and that the two adjacent segments work together as a phosphoSIM.

Like PML, a number of other proteins that transit into PML-NBs, including Daxx and PIAS1, contain a phosphoSIM module, and their noncovalent interaction with SUMO proteins are known to be regulated in a phosphorylation-dependent manner (Cho et al., 2009; Lin et al., 2006; Negorev et al., 2001; Rasheed et al., 2002; Sung et al., 2011). Based on studies analyzing interactions between SUMO proteins and phosphoSIM-containing proteins, it has been postulated that the phosphorylated residues make contacts with positively charged surface residues that are conserved in SUMO family proteins (Chang et al., 2011; Sekiyama et al., 2008; Song et al., 2005; Stehmeier and Muller, 2009; Ullmann et al., 2012). In the case of SUMO1, it has been suggested that K37, K39, H43, K45, and K46 may make important contacts based on mutational analysis. In addition, it has been demonstrated that the interaction between phosphoSIMs and SUMO family proteins may be further regulated in a posttranslational manner through acetylation of SUMO family proteins at several of these same lysine residues (Cheema et al., 2010; Choudhary et al., 2009; Ullmann et al., 2012). In particular, SUMO1 acetylated at K37 (K33 in SUMO2) displayed a decreased affinity for the phosphoSIMs of numerous proteins (Ullmann et al., 2012).

Given the important role that phosphorylation of PML plays in regulating its function, we have used a combination of functional, biochemical, and structural studies to characterize the interaction between the phosphoSIM of PML and SUMO1 at the atomic level. We establish that the interaction between SUMO1 and PML is strongly enhanced by phosphorylation of the four serine residues of the phosphoSIM of PML. Structural characterization of SUMO1 in complex with a phosphoSIM peptide of PML in both its unphosphorylated and tetraphosphorylated forms indicates that three of the four phosphoserine residues directly interact with positively charged residues of SUMO1, and mutation of these positively charged residues within SUMO1 significantly decreases its interaction with PML in human cells. In addition, structural characterization of a phosphoSIM peptide of Daxx in both its unphosphorylated and diphosphorylated forms indicates that the hydrophobic residues have similar interactions, but the acidic/phosphorylated residues have different interactions with SUMO1. Together, these results provide an atomic level description of the role of phosphorylation of PML in PML interaction with SUMO proteins, as well as important insights into how different spacing patterns of acidic/phosphorylated residues within phosphoSIMs can interconnect with the acetylation patterns of the different SUMO family proteins to define specificity.

RESULTS

Blocking Phosphorylation of PML Decreases Noncovalent Binding to SUMO Proteins in Cells

Previous studies have shown that four serine residues (S560, S561, S562, and S565 in PML-I) in the phosphoSIM of PML are phosphorylated and substituting these residues with aspartic acid enhanced PML binding to SUMO1 (Percherancier et al., 2009; Scaglioni et al., 2006; Stehmeier and Muller, 2009; Rabellino et al., 2012). In addition, the phosphoSIM of PML is conserved in most PML isoforms and several other proteins found in PML-NBs have similar phosphoSIM sequences (Figure 1A; Figure S1 available online). To confirm the role of the PML phosphoSIM for noncovalent binding to SUMO1 in human cells, we measured the interaction between wild-type PML, a nonphosphorylable mutant of PML (PML-4SA; four serines mutated to alanines), and a phosphomimetic mutant of PML (PML-4SD; four serines mutated to aspartic acid) with a nonconjugable version of SUMO1 (GFP-SUMO1; two C-terminal glycines mutated to alanine) using bioluminescence resonance energy transfer (BRET) (Figure 1B).

HEK293T cells were cotransfected with a fixed quantity of DNA coding for either the wild-type PML (PML-Rluc), the nonphosphorylable mutant (PML-4SA-RLuc), or the phosphomimetic mutant (PML-4SD-Rluc) fused to Renilla luciferase along with increasing amounts of a DNA coding for GFP-SUMO1. For wild-type PML, the BRET ratio increased as a function of GFP-SUMO1 concentration and reached a maximum when the GFP-SUMO1 expression levels were no longer limiting relative to the PML-Rluc expression levels (Figure 1C). The saturation curve indicated a specific noncovalent interaction between PML and SUMO1 under our experimental conditions, since the GFP-SUMO1 was nonconjugable. In contrast, a significantly lower BRET signal was obtained for the interaction between PML-4SA-Rluc and GFP-SUMO1 (Figure 1C). This indicated a weaker interaction between PML-4SA and SUMO1 and suggested that phosphorylation events targeting the serine residues of PML could be modulating the SUMO1:PML noncovalent interactions. Next, we measured the interaction between SUMO1 and the phosphomimetic PML mutant. A BRET saturation curve similar to the one of the wild-type PML was obtained between PML-4SD-Rluc and GFP-SUMO1 (Figure 1C). This result demonstrated that replacing the alanine residues with the negatively charged aspartic acid restored the ability of PML to interact with SUMO1 in HEK293T cells. Moreover, it suggested that the serine residues within the SIM module of PML may be phosphorylated in HEK293 cells. This would be consistent with previous studies demonstrating that the fourth serine (S565) within the phosphoSIM of PML is significantly phosphorylated in HEK293 cells, and that phosphorylation at S565 triggers the subsequent phosphorylation of positions S560, S561, and S562 (Scaglioni et al., 2006;Rabellino et al., 2012).

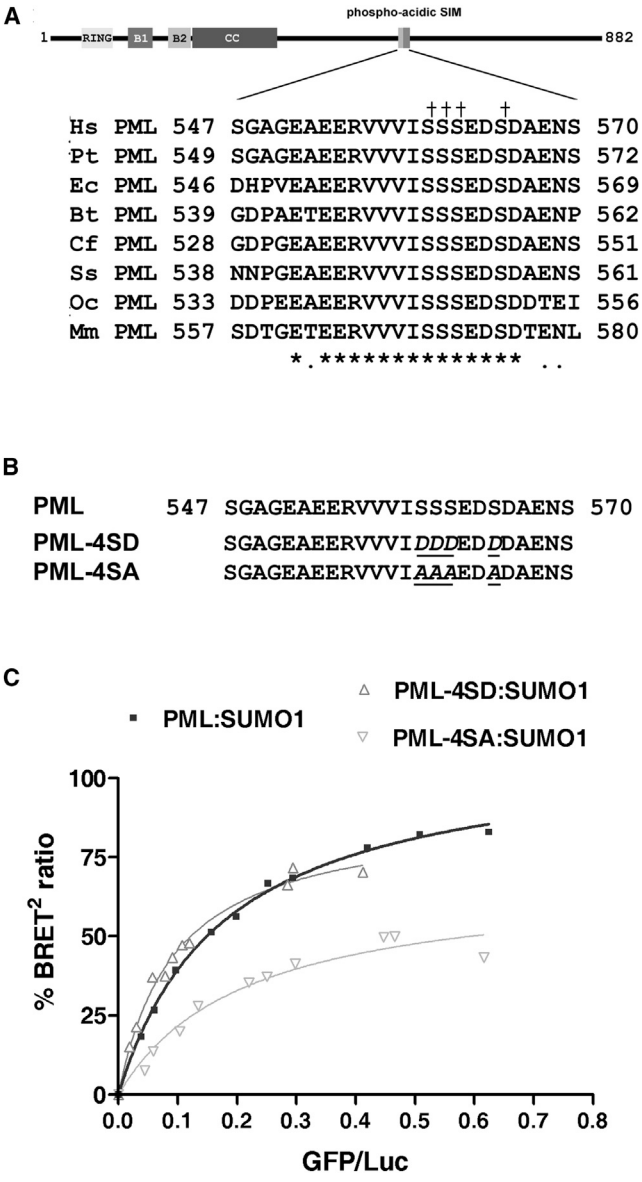

Figure 1. Interaction between SUMO1 and PML in HEK293T Cells

(A) Schematic representation of PML domains (human PML-I) and sequence alignment of the phosphoSIM regions of PML from different eukaryotic species. The domains and regions indicated as boxes in the schematic representation include the Really Interesting New Gene (RING) domain (light gray), the B1 and B2 B-box domains (medium gray), the coiled-coil domain (dark gray), and the phosphoSIM module (black). In the alignment of the PML phosphoSIM region: †, CK2-concensus sites; *, identical residues in the aligned sequences; and ., homologous residues.

(B) Amino-acid sequence of phosphoSIM mutants used for BRET studies. The residues mutated are in italics and underlined.

(C) Representative BRET titration curves showing interaction between SUMO1 and either wild-type PML or mutants in HEK293T cells. The PML-RLuc (■), PML-4SD-Rluc (△), and PML-4SA-Rluc (▽) were used with GFP-SUMO1. See also Figure S1.

Phosphorylation of PML SIM Enhances Binding to SUMO1 In Vitro

As the BRET results supported previous studies suggesting that phosphorylation of the phosphoSIM in PML modulates its interaction with SUMO1 (Percherancier et al., 2009; Scaglioni et al., 2006; Stehmeier and Muller, 2009; Rabellino et al., 2012), we attempted to quantitatively address the role that phosphorylation has on the binding of PML to SUMO1 in vitro. For these studies, two peptides corresponding to residues 547–573 of PML-I were prepared and their apparent dissociation constants (K_D) for binding to SUMO1 measured by isothermal titration calorimetry (ITC) (Figure 2A). These peptides encompass the phosphoSIM including both the hydrophobic region (V556, V557, V558, and I559) and the serine residues (560, 561, 562, and 565) that are phosphorylated in PML (Figure 2B). The first peptide contained the wild-type PML sequence (PML-SIM), whereas in the second peptide S560, S561, S562, and S565 were phosphorylated (PML-SIM-PO_4). In the ITC assay, the PML-SIM peptide bound SUMO1 with a K_D of 44 ± 5 μM, whereas the PML-SIM-PO_4 peptide bound with a 37-fold higher affinity and a K_D of 1.2 ± 0.2 μM (Figure 2C). Taken together, the in vitro ITC results strongly support that phosphorylation of the four serine residues present in the phosphoSIM of PML significantly enhances the noncovalent binding of PML to SUMO1.

SUMO1 Lysine Residues Are Essential for the SUMO1:PML Interaction

As mentioned above, the region of SUMO1 spanning from the end of β2 to the start of the α1 contains two positively charged patches that are conserved in all SUMO proteins and have been shown to be important for binding to phosphoSIM motifs (Chang et al., 2011; Sekiyama et al., 2008; Song et al., 2005; Stehmeier and Muller, 2009; Ullmann et al., 2012). The first positively charged patch of SUMO1 includes K37 and K39 and the second patch contains K45 and K46 (Figure 3A). To determine the importance of positively charged residues for SUMO1 binding to full-length PML in human cells, we generated a series of lysine to alanine mutants within these two positively charged patches of SUMO1 [SUMO1-K37A-K39A, SUMO1-K45A-46A and SUMO1-K37A-K39A-K45A-K46A (SUMO1-4KA)] and tested their ability to bind PML using our BRET assay. In comparison to the BRET signal observed between wild-type PML-RLuc and GFP-SUMO1, a significant decrease was observed in the BRET signals for the interactions between PML-RLuc and either the GFP-SUMO1-K37A-K39A, GFP-SUMO1-K45A-K46A, or GFP-SUMO1-4KA mutant in HEK293T cells (Figure 3B). Interestingly, the decrease in the intensity of the BRET signal was similar for the three mutants tested, and this suggested that the two basic patches function in unison to achieve optimal binding to PML with the four lysine residues of SUMO1, contributing in both direct and indirect manners.

K39, H43, and K46 of SUMO1 Contact with the PML-SIM-PO_4 Peptide

To more precisely identify positively charged residues of SUMO1 that specifically interact with the phosphorylated serine residues in the PML-SIM-PO_4 peptide, chemical shift perturbation studies were performed using nuclear magnetic resonance (NMR) spectroscopy. In these studies, ^{1}H-^{15}N heteronuclear single quantum coherence (HSQC) experiments were conducted with ^{15}N-labeled SUMO1 and either the PML-SIM peptide or the PML-SIM-PO_4 peptide. As expected, the sequential addition of either peptide resulted in changes in both the ^{1}H and ^{15}N chemical

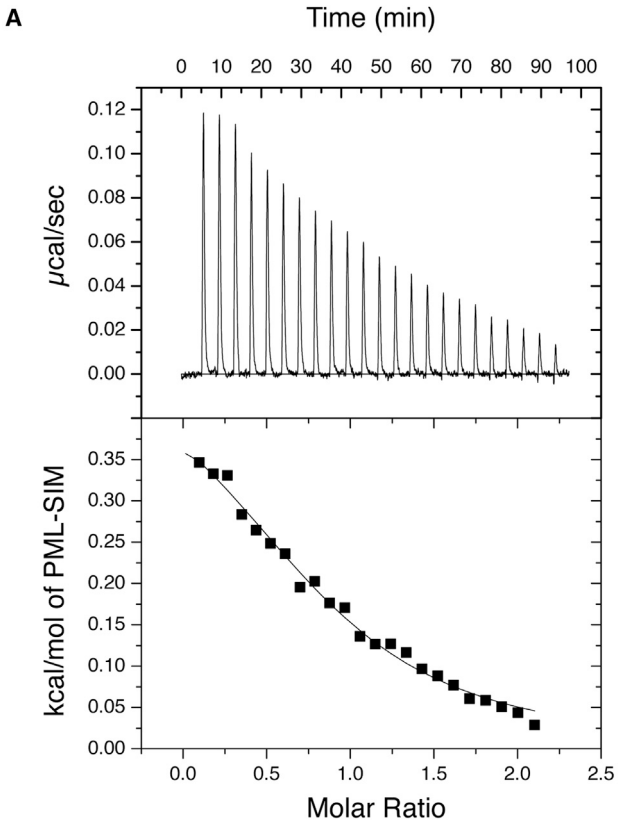

B

PML-SIM SGAGEAEERVVVIS S S EDS DAENSSSR
PML-SIM-PO_4 SGAGEAEERVVVI**S**$_{PO4}$**S**$_{PO4}$**S**$_{PO4}$ED**S**$_{PO4}$DAENSSSR

C

Peptide	PML-SIM	PML-SIM-PO4
K_D (μM)	44.5 ± 5 μM	1.2 ± 0.2 μM

Figure 2. Phosphorylation of PML Enhances Interaction with SUMO1

(A) Representative ITC thermogram for the interaction between SUMO1 and the PML-SIM peptide.

(B) Amino-acid sequences of the PML-SIM and the PML-SIM-PO_4 peptides used in the ITC studies.

(C) Comparison of the dissociation constant (K_D) values for SUMO1 binding to the PML-SIM and PML-SIM-PO_4 peptides in the ITC studies.

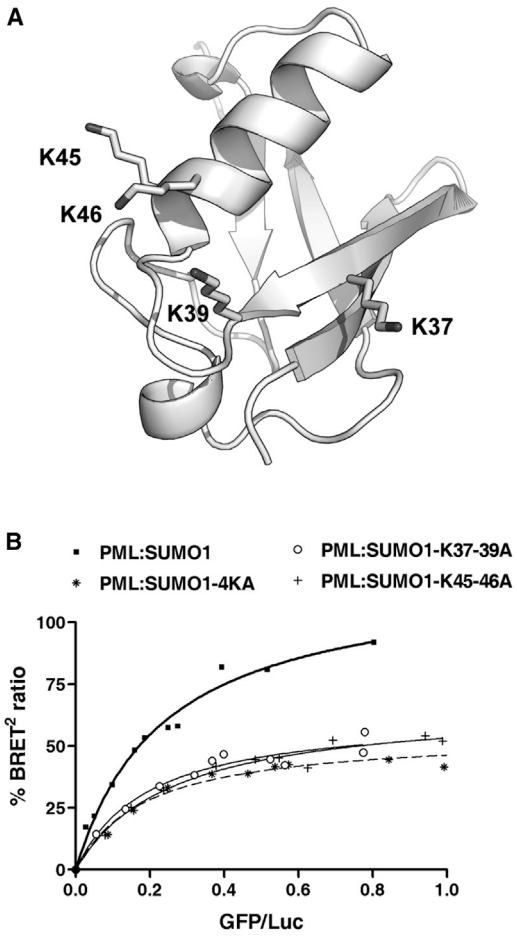

Figure 3. SUMO1 Lysine Residues Are Critical for PML:SUMO1 Interaction

(A) Ribbon model of the 3D structure of SUMO1 (light gray; PDB ID 2UYZ) with lysine residues from the two basic patches highlighted as sticks.

(B) Representative BRET titration curves showing interaction between either wild-type SUMO1 or the SUMO1 basic patch mutants and PML in HEK293T cells. PML-RLuc was used with GFP-SUMO1 (■), GFP-SUMO1-K37-39A (○), GFP-SUMO1-K45-46A (+), or GFP-SUMO1-4KA (*).

shifts for several signals of SUMO1 (Figure S2). Superimposition of the ^{1}H-^{15}N HSQC spectra from the two titrations after the addition of one equivalent of peptide revealed several important differences (Figure 4A). These differences indicated that specific chemical shift perturbations were occurring in SUMO1 upon interaction with the PML-SIM-PO_4 peptide (Figure 4B) due to the presence of the phosphoserine residues. The most significant differences occured at signals corresponding to residues located primarily in the region of SUMO1, spanning from the end of its second β strand (β2) to the middle of its α helix (α1) (Figures 4B and 4C). This region of SUMO1 includes the two positively charged patches, and K39, H43, and K46 within this region showed the most dramatic differences when comparing the ^{1}H-^{15}N HSQC spectra obtained with the PML-SIM peptide with that of the PML-SIM-PO_4 peptide (Figure 4B). Interestingly, these results are similar to what was observed in NMR studies between SUMO1 and peptides corresponding to the phosphoSIM of Daxx, where the most dramatic chemical shift changes following phosphorylation were observed for V38, K39, and H43 (Chang et al., 2011). Consistent with the BRET and ITC studies, the NMR chemical shift perturbation studies supported the notion that phosphorylation of the phosphoSIM from PML enhances its affinity for SUMO1 and that phosphorylated residues from the phosphoSIM of PML contact a number of positively charged amino acids in SUMO1.

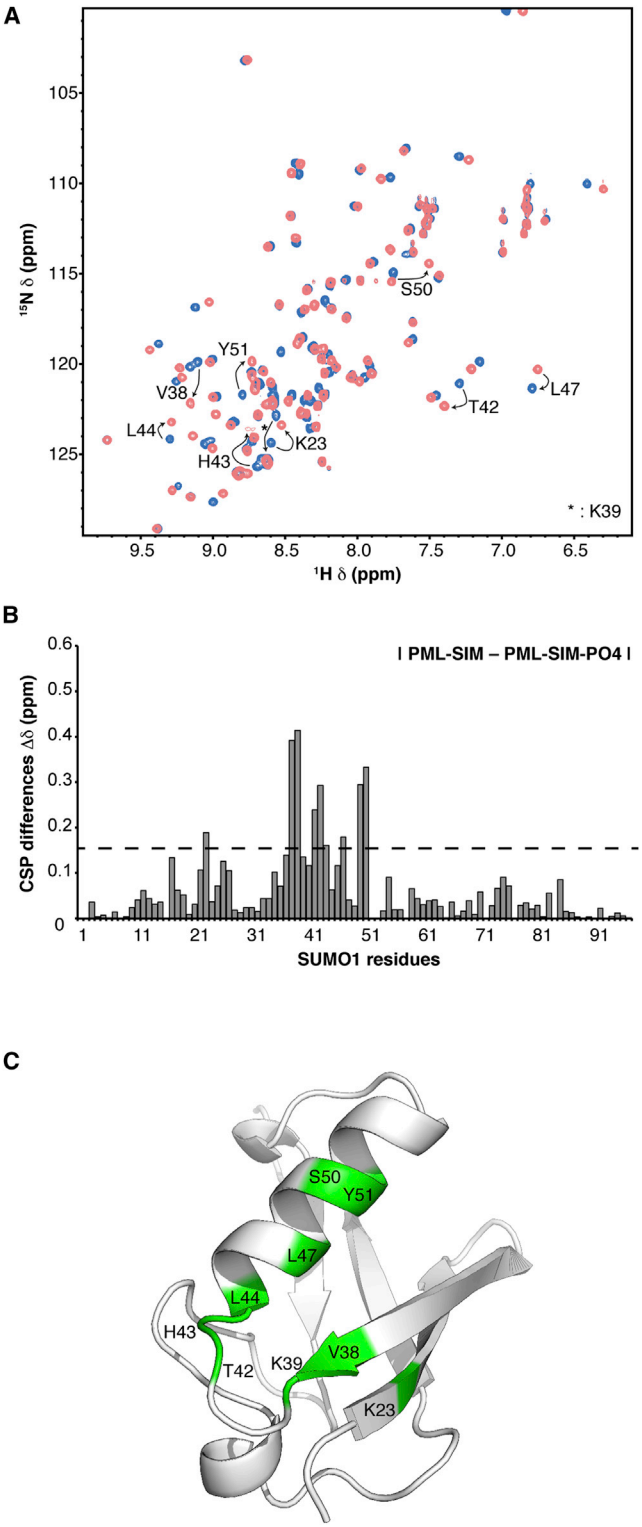

Figure 4. Positively Charged Residues in SUMO1 Make Specific Interactions with the PML-SIM-PO$_4$ Peptide

(A) Overlay from the 2D ^{1}H-^{15}N HSQC spectra of ^{15}N-labeled SUMO1 in the presence of one molar equivalent of either the unlabeled PML-SIM (blue) or PML-SIM-PO$_4$ peptide (pink).

(B) Histogram of the differences in chemical shift perturbations (CSP) that occur in the titration between ^{15}N-labeled SUMO1 and the PML-SIM-PO$_4$ peptide with those obtained in the titration between ^{15}N-labeled SUMO1 and the PML-SIM peptide. The differences in chemical shift changes for the two individual titrations were calculated using the formula $\Delta\delta = [(0.17\Delta N_H)^2 + (\Delta H_N)^2]^{1/2}$.

(C) Ribbon model of the 3D structure of SUMO1 (light gray; PDB ID 2UYZ). The amino acids of ^{15}N-labeled SUMO1 showing a significant chemical shift change ($\Delta\delta$ [ppm] > 0.15) upon formation of a complex with PML-SIM-PO$_4$ are highlighted in green.

See also Figure S2.

Structure of the SUMO1:PML-SIM-PO$_4$ Complex

To gain structural insights into the role that phosphorylation of the phosphoSIM of PML has on its noncovalent interaction with SUMO1, we crystallized an N-terminal truncated form of SUMO1 (ΔN-SUMO1; residues 17–97 of human SUMO1) in complex with the PML-SIM-PO$_4$ peptide. The crystals belong to the $P2_12_12_1$ space group, diffract to a resolution of 1.50 Å, and contain one ΔN-SUMO1:PML-SIM-PO$_4$ complex in the asymmetric unit (Table 1). Clear density was visible for residues 18–94 of SUMO1, residues 552–562 (Figure 5), and 569–573 (Figure S3) of PML. In complex with the PML-SIM-PO$_4$ peptide, SUMO1 adopted a canonical ubiquitin-like fold, whereas the PML-SIM-PO$_4$ peptide adopted a parallel β strand conformation with respect to the second β strand (β2) of SUMO1 (Figure 5B). This portion of the β sheet was stabilized by a network of hydrogen bonds between the backbone of PML (residues 555–559) and the backbone of SUMO1 (residues 35–37). In this configuration, the side chains of PML residues V556 and V558 were partially exposed to the solvent, whereas those of residues V557 and I559 were buried within a hydrophobic groove of SUMO1 composed of the α1 helix and the β2 strand. The hydrophobic region of the phosphoSIM was stabilized by contacts with the side chains of Y21, K23, I34, H35, F36, K37, V38, K46, L47, and R54 from SUMO1. In addition, the residues immediately N-terminal to the hydrophobic region (E554 and R555) provided additional contacts to SUMO1. Notably, the Nε atom of R555 of PML formed a hydrogen bond with the backbone of E33 from SUMO1, while the terminal guanidino group participated in a water-mediated hydrogen bond network with SUMO1.

Consistent with the results from the BRET, ITC, and NMR studies, the three phosphoserine residues (S560, S561, and S562) immediately adjacent to the hydrophobic region were visible in the electron density maps (Figure 5A), and the phosphate moiety of each residue was making contact with SUMO1 residues in the complex (Figure 5B). More precisely, the phosphate moiety of S560 formed a hydrogen bond with K46, the phosphate moiety of S561 formed an electrostatic interaction with K39, and the phosphate moiety of S562 formed hydrogen bonds with H43. In contrast, the fourth serine residue (S565) did not appear to be stabilized by interactions with SUMO1 in the crystal structure, but previous studies have shown that it is crucial for the subsequent phosphorylation of S562 by CK2 (Scaglioni et al., 2006).

To verify that the phosphates groups of PML specifically contribute to binding to SUMO1, we obtained crystals of the same SUMO1 construct in complex with the PML-SIM peptide in the unphosphorylated form. The crystals of the ΔN-SUMO1:PML-SIM complex belong to the same $P2_12_12_1$ space group and diffract to a resolution of 1.46 Å (Table 1). In contrast to

Table 1. Data Collection and Refinement Statistics

Data Set	SUMO1:PML-SIM-WT	SUMO1:PML-SIM-PO_4	SUMO1:DAXX-SIM-WT	SUMO1:DAXX-SIM-PO_4
Data Collection				
Beamline	X29, NSLS	08-ID, CLS	X25, NSLS	X25, NSLS
Wavelength (Å)	1.075	0.9794	1.100	1.100
Space group	$P2_12_12_1$	$P2_12_12_1$	$P2_1$	$P2_1$
Unit-cell parameter (Å)	A = 38.39, b = 47.25, c = 63.91	a = 38.27, b = 47.08, c = 63.98	a = 34.64, b = 38.40, c = 73.69, β = 101.09	a = 34.27, b = 38.07, c = 73.95, β = 101.04
Resolution (Å)	50-1.46 (1.54–1.46)	50-1.50 (1.58–1.50)	50-1.35 (1.42–1.35)	50-1.70 (1.79–1.70)
No. of unique reflections	20,770	18,558	39,759	20,835
Multiplicity	6.8 (5.6)	9.8 (6.0)	3.1 (2.1)	3.3 (3.3)
Completeness (%)	99.2 (95.4)	96.9 (81.8)	94.6 (74.6)	99.9 (100.0)
R_{merge}	0.092 (0.597)	0.112 (0.870)	0.036 (0.366)	0.042 (0.412)
$I/\sigma(I)$	11.6 (2.7)	11.5 (2.1)	16.1 (2.4)	15.3 (2.6)
Refinement Statistics				
Resolution (Å)	50-1.46	50-1.50	50-1.35	50-1.70
Reflections (total/test)[a]	20,720/1,037	18,509/926	39,748/2,005	20,821/1,051
R_{work}/R_{free} (%)	15.66/18.38	15.83/19.21	15.58/18.09	16.28/19.52
No. of atoms (excluding hydrogens)				
Protein	752	782	1,442	1,476
Water	148	146	333	177
B factors				
Protein	18.69	19.64	21.57	34.02
Water	36.15	37.86	35.69	42.33
Rmsds				
Bond lengths (Å)	0.010	0.010	0.009	0.012
Bond angles (°)	1.363	1.298	1.235	1.253
Ramachandran[b]				
Favored (%)	100.0	100.0	97.1	98.2
Outliers (%)	0	0	0	0

Values in parentheses are for highest resolution shell. $R_{sym} = \sum hkl \sum i |I_{hkl,i} - < Ihkl > | / \sum_{hkl,i} < Ihkl >$, where $I_{hkl,i}$ is the intensity of an individual measurement of the reflection with Miller indices *hkl* and I_{hkl} is the mean intensity of that reflection. $R_{work} = \sum hkl \parallel F_o| - |F_c \parallel / \sum hkl |F_o|$, where $|F_o|$ is the observed structure-factor amplitude and $|F_c|$ is the calculated structure-factor amplitude. R_{free} is the R factor based on at least 500 test reflections that were excluded from the refinement.
[a]Reflections with $F_o > 0$.
[b]MolProbity analysis.

what was observed in the structure of the ΔN-SUMO1:PML-SIM-PO_4 complex, where the four phosphoserine residues were visible in the electron density maps, S560 was the only serine residue visible in the electron density map of the SUMO1:PML-SIM complex (Figure 5C). In addition, we did not observe an interaction between S560 of PML and K46 of SUMO1 (Figure 5D); this indicated that phosphorylation effectively contributes to the stabilization of the serine residues adjacent to the hydrophobic residues of the phosphoSIM of PML. As expected, the positions of the four hydrophobic residues of the phosphoSIM were identical in both complexes, and this was in good agreement with previous structural studies describing the mode of interaction of the four hydrophobic residues of SIMs (Armstrong et al., 2012; Chang et al., 2011; Reverter and Lima, 2005; Sekiyama et al., 2008; Song et al., 2005). Importantly, the specific interactions involving the three phosphoserine residues in the SUMO1:PML-SIM-PO_4 structure were consistent with the BRET, ITC, and NMR data, which indicated that PML phosphorylation increases its affinity for SUMO1 and highlighted the roles that K39, H43, and K46 of SUMO1 contribute to the binding interface.

The Hydrophobic and Serine Residues of the PhosphoSIM Both Impact PML Tumor Suppression Function

To assess whether PML tumor suppression activity is affected by the affinity of the phosphoSIM for SUMO proteins and/or SUMOylated partners, we generated mutations in either the hydrophobic (PML-VVVI-AAAS: the SIM hydrophobic residue mutations of amino acids 556–559) or serine (PML-4SA) residues of the phosphoSIM. The mutations were introduced into the PML-IV isoform, since this is the only isoform known to induce senescence (Bischof et al., 2002). To test the activity of the PML phosphoSIM mutants, we chose the human osteosarcoma cell line U2OS, a cell line in which PML-IV has been shown to act as a tumor suppressor (Vernier et al., 2011). Our results showed

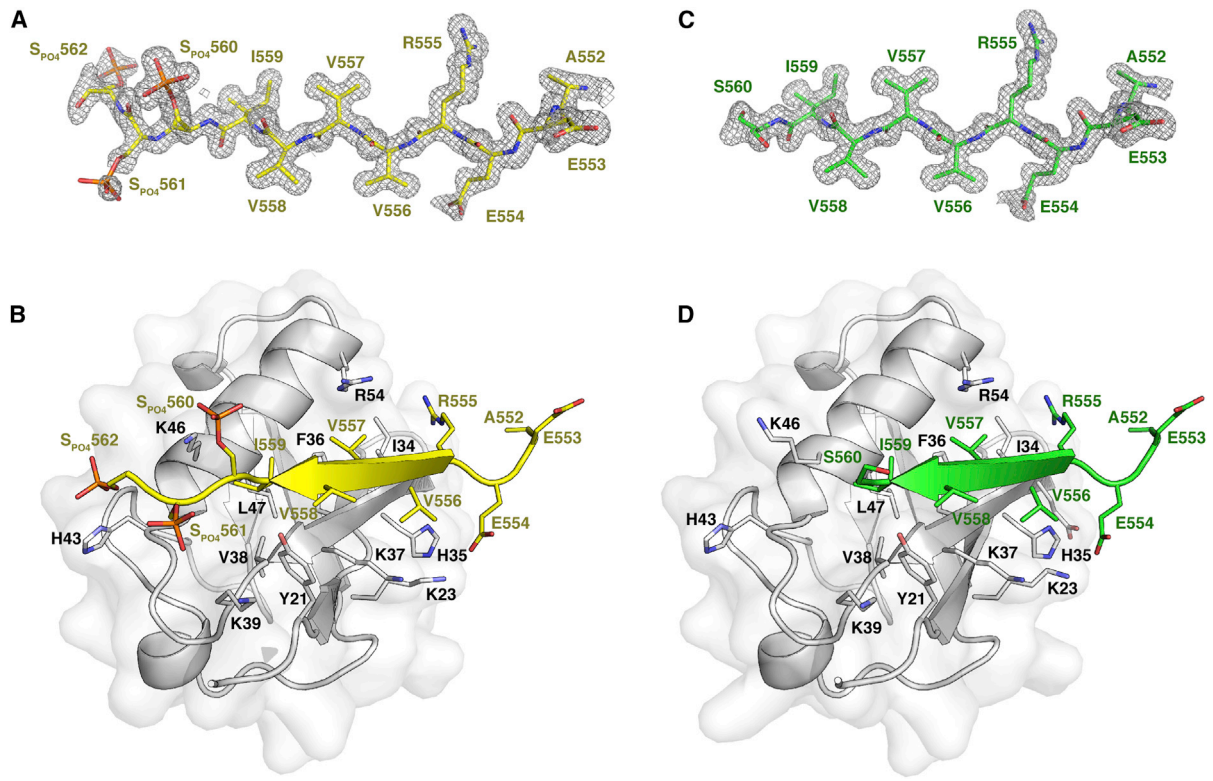

Figure 5. Crystal Structures of the ΔN-SUMO1:PML-SIM-PO_4 and ΔN-SUMO1:PML-SIM Complexes

(A) Electron density map corresponding to residues 552–562 of PML-SIM-PO_4. The peptide is in stick representation with carbon atoms colored in yellow. The $2F_oF_c$ electron density map, contoured at 0.8σ, is represented by a gray mesh.

(B) Overall structure of the ΔN-SUMO1:PML-SIM-PO_4 complex highlighting the interactions between SUMO1 and residues 552–562 of PML (PDB entry 4WJN). The proteins are in cartoon representation with ΔN-SUMO1 carbon atoms (gray) and PML-SIM-PO_4 peptide carbon atoms (yellow); ΔN-SUMO1 residues interacting with the PML-SIM-PO_4 peptide are in stick representation.

(C) Electron density map corresponding to PML-SIM residues 552–560 and using the same representation mode as in (A) with PML carbon atoms colored in green.

(D) Overall structure of the ΔN-SUMO1:PML-SIM complex highlighting the interactions between SUMO1 and PML (PDB entry 4WJO). The presentation is similar to (C) with PML carbon atoms colored in green.

See also Figure S3.

that, upon stable exogenous expression of PML-IV in U2OS cells, growth was slower than in U2OS expressing only the empty vector (Figure 6A). Surprisingly, expression of either of the two PML-IV phosphoSIM mutants demonstrated an increased repressive effect on U2OS growth in comparison to wild-type PML-IV (Figure 6A). However, this difference in growth was not a direct consequence of expression levels of the proteins in the established U2OS cell lines, as neither phosphoSIM mutant displayed a higher steady-state expression level compared with the wild-type PML-IV protein (Figure 6B).

Since examining the form and number of the PML-NBs is often used to assess the functionality of PML, we performed immunofluorescence studies against PML in the U2OS cell lines expressing the control vector, wild-type PML-IV, the PML-VVVI-AAAS mutant, or the PML-4SA mutant. In all cases, overexpression of the PML proteins (along with the endogenous PML) resulted in an increase in both the number and the size of the PML-NBs in the cell nucleus (Figure 6C). Interestingly, the most dramatic increases appeared to be with the two phosphoSIM mutants of PML. Overall, the results demonstrated that lowering the potential of the phosphoSIM of PML to interact with SUMO and/or SUMOylated proteins does alter the tumor suppression effects of PML-IV without preventing formation of PML-NBs in cancer cells expressing endogenous PML. Of note, only nonsumoylatable PML-IV mutants have been shown previously to maintain tumor suppression activity (Bischof et al., 2002), but our results demonstrated that PML phosphoSIM binding is also not required and can be modulated.

Structure of the SUMO1:Daxx-SIM-PO_4 Complex

Several proteins that are found in PML-NBs contain a phosphoSIM similar to the one found in PML (Figure S1B; Cho et al., 2009; Lin et al., 2006; Rasheed et al., 2002; Sung et al., 2011). In the case of Daxx, it has been shown that phosphorylation of two serine residues in its phosphoSIM motif increases its binding affinity to SUMO1 and plays a key role in regulating a number of its biologic functions (Chang et al., 2011). To determine whether the phosphorylation state of the phosphoSIM of Daxx affects its binding to SUMO1 in a manner similar to that observed for PML, we attempted to solve the structure of a peptide from the

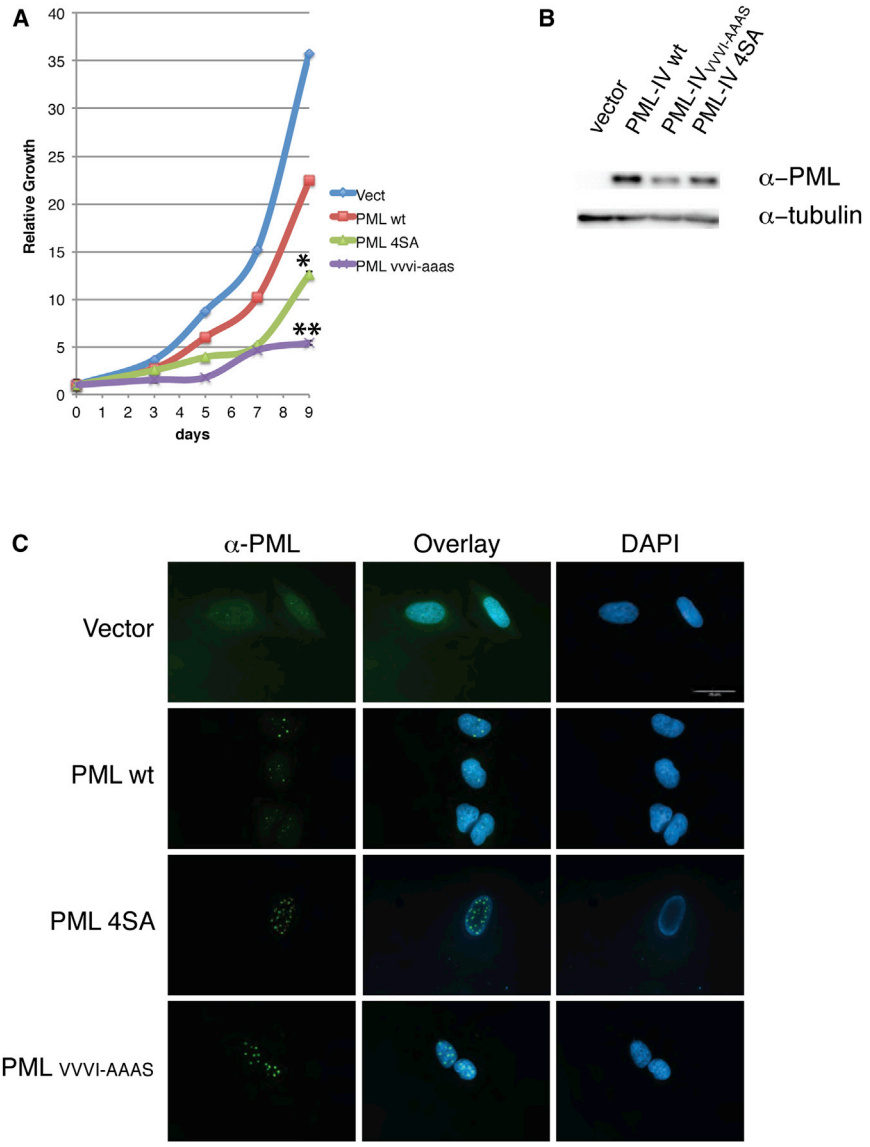

Figure 6. In Vivo Effect of Expressing PML-IV Wild-Type or PhosphoSIM Mutants in U2OS Cells

(A) Growth curves for U2OS cells stably expressing a control (Vect), a PML-IV (PML-wt), a PML-4SA mutant, or a PML-VVVI-AAAS mutant. Data are represented as mean of triplicates monitored over a 9-day growth period, and statistical analysis (t test) for the mutants was performed relative to the PML-wt. * $p < 5 \times 10^{-4}$, ** $p < 5 \times 10^{-5}$.

(B) Immunoblots of PML and tubulin in U2OS cells as in (A).

(C) Indirect immunofluorescence with an anti-PML antibody and DAPI, nuclear marker, to visualize PML-NBs in U2OS cells, as in (A).

phosphoSIM of Daxx bound to SUMO1. The phosphoSIM of Daxx (residues 733–740) is composed of an I-I-V-L hydrophobic sequence immediately followed by an S-D-S-D sequence, where the two serine residues are CK2 substrates (Chang et al., 2011). The structure of a SUMO1-Daxx-SIM peptide complex in the unphosphorylated state has been characterized previously by NMR spectroscopy. In addition, ITC studies demonstrated that phosphorylation of the two serine residues increases the affinity of the Daxx-SIM peptide for SUMO1 55-fold (Chang et al., 2011).

Initial attempts to crystallize either SUMO1 or ΔN-SUMO1 in complex with a Daxx-SIM peptide in either the phosphorylated or unphosphorylated state were unsuccessful. Careful examination of the crystal structures of ΔN-SUMO1 bound to the PML-SIM peptides suggested that five residues at the N terminus of the PML peptides established contacts that helped stabilize the crystal lattice. We therefore created a modified version of the Daxx-SIM peptide, termed mDaxx-SIM, containing the five residues from PML that make the crystal contacts as an N-terminal tag. Importantly, this strategy allowed for the crystallization of both a ΔN-SUMO1:mDaxx-SIM-PO_4 and a ΔN-SUMO1:mDaxx-SIM complex (Table 1; Figure S4). The ΔN-SUMO1:mDaxx-SIM-PO_4 crystals diffracted to 1.70-Å resolution, belong to the $P2_1$ space group, and contain two ΔN-SUMO1:mDaxx-SIM-PO_4 complexes in the asymmetric unit. Residues 733 to 740 of mDaxx-SIM-PO_4 peptide were visible in one subunit, whereas only residues 733 to 737 were visible in the other. Likewise, the ΔN-SUMO1:mDaxx-SIM crystals diffracted to 1.35-Å resolution, belong to the $P2_1$ space group, and contain two ΔN-SUMO1:mDaxx-SIM complexes in the asymmetric unit. However, in both subunits only residues 733 to 737 of the mDaxx-SIM peptide were visible.

The structures of the mDaxx-SIM-PO_4 and mDaxx-SIM peptides in complex with SUMO1 presented several similitudes with the structures of the PML-SIM-PO_4 and PML-SIM peptides bound to SUMO1. As expected, the hydrophobic portions of the mDaxx-SIM peptides adopted similar conformation to the corresponding portion of the PML-SIM peptides, and the same residues that stabilized the phosphoSIM of PML also stabilized the phosphoSIM of Daxx (Figure 7A). Moreover, the two phosphoserines (S737 and S739) of the Daxx-SIM-PO_4 peptide occupied similar positions as the first (S560) and third (S562) phosphoserines of the PML-SIM-PO_4 peptide (Figure 7B). However, K46 of SUMO1 did not seem to have a specific role in stabilizing the S737 phosphoserine of the mDaxx-SIM-PO4 peptide, as was seen with S560 phosphoserine of PML, but rather it appeared to provide a generally favorable environment for the presence of both phosphoserines while accommodating the bulkier hydrophobic region of the Daxx phosphoSIM through its aliphatic moiety. The structures of the PML-SIM-PO_4 and mDaxx-SIM-PO_4 peptides bound to SUMO1 also differed noticeably with respect to the position of the negatively charged residue in position two after the hydrophobic residues.

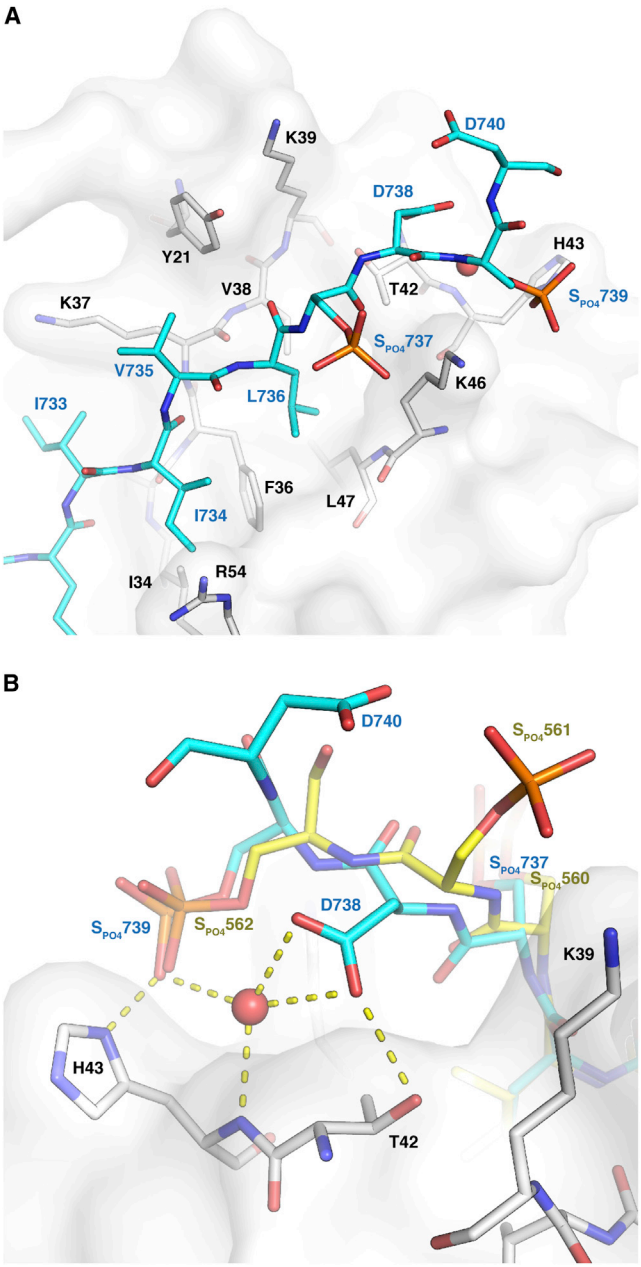

Figure 7. Structural Comparison of the ΔN-SUMO1:PML-SIM-PO_4 and ΔN-SUMO1:mDaxx-SIM-PO_4 Complexes

(A) Structure of the ΔN-SUMO1:mDaxx-SIM-PO_4 complex highlighting the interactions between SUMO1 and residues 733–740 of Daxx (PDB entry 4WJP). The proteins are in cartoon representation with ΔN-SUMO1 carbon atoms (gray) and mDaxx-SIM-PO_4 peptide carbon atoms (cyan); ΔN-SUMO1 residues interacting with mDaxx-SIM-PO_4 are in stick representation.

(B) Structural comparison of the phosphorylated/acidic region of the phosphoSIMs of PML and Daxx (cyan) in the phosphorylated form. The proteins are in cartoon representation with the ΔN-SUMO1 carbon atoms (gray), the PML-SIM-PO_4 peptide carbon atoms (yellow), and the mDaxx-SIM-PO_4 peptide carbon atoms (cyan); ΔN-SUMO1 residues interacting with the mDaxx-SIM-PO_4 peptide are in stick representation.

See also Figure S4.

The second phosphoserine (S561) of the PML-SIM-PO_4 peptide was stabilized by an interaction with the positive charge from K39 of SUMO1, whereas D738 in the equivalent position in mDaxx-SIM-PO_4 peptide was at hydrogen bond distance from both the hydroxyl group of T42 of SUMO1 and a water molecule (Figure 7B). Interestingly, this water molecule also was coordinated by the backbone amide of T42 and by the phosphate moiety of the second phosphoserine of the mDaxx-SIM-PO_4 peptide. Based on these structures, it appeared that, in their phosphorylated form, the phosphoSIM of Daxx was bound to SUMO1 through a similar but not identical mechanism compared to the phosphoSIM of PML. This suggests that subtle spacing patterns of the acidic and serine residues within phosphoSIMs can play an important role in their binding to SUMO proteins (Figure S1B).

DISCUSSION

Despite the important functional role of phosphoSIMs in several proteins, very little is known about how the phosphorylated amino acids within the phosphoSIM enhance the binding affinity for SUMO proteins at the atomic level (Chang et al., 2011; Stehmeier and Muller, 2009). Using PML as a model, we have characterized the role phosphorylation plays in the binding of the phosphoSIM of PML to SUMO1 at the atomic level using a combination of functional, biophysical, and structural studies. We established that PML binding to SUMO1 is strongly enhanced by phosphorylation of four serine residues within the phosphoSIM of PML. Consistent with the increased binding affinity observed both in vivo with full-length PML and in vitro with a PML-SIM-PO_4 peptide, the crystal structures of the SUMO1:PML-SIM-PO_4 and SUMO1:PML-SIM complexes revealed that three phosphorylated serine residues within the PML-SIM-PO_4 peptide make specific contacts with positively charged residues on the surface of SUMO1. We also demonstrated that both the hydrophobic residues and the phosphorylated residues within the phosphoSIM of PML function in unison to regulate both the tumor suppression properties of PML and PML-NB formation. In addition, the crystal structure of the SUMO1:mDaxx-SIM-PO4 complex with SUMO1 indicates that in its phosphorylated form the phosphoSIM of Daxx makes similar but nonidentical contacts at the interface with SUMO1 as those observed for the phosphoSIM of PML.

Our structures of the SUMO1:PML-SIM-PO_4 and SUMO1:PML-SIM complexes provide an atomic level description into the role that phosphorylation plays in the binding of the phosphoSIM of PML to SUMO1. Comparison of these peptide complexes to previously characterized SUMO:SIM-containing complexes revealed both similarities and differences between the PML phosphoSIM and other canonical SIMs. Like several canonical SIMs, the hydrophobic core of the PML phosphoSIM contacted hydrophobic residues in a groove of SUMO1 and adopted a parallel orientation with respect to the β2 strand of SUMO1 (Armstrong et al., 2012; Olsen et al., 2010; Reverter and Lima, 2005; Sekiyama et al., 2008; Song et al., 2005). In addition, the hydrophobic portion of the SIM sequence was followed immediately by a cluster of serine and/or negatively charged residues that did not strongly participate in the stabilization of the interaction with SUMO1 in the unphosphorylated SUMO1:PML-SIM

complex (Chang et al., 2011; Sekiyama et al., 2008; Song et al., 2005).

This is consistent with previous NMR structures of the SUMO1:PIAS2-SIM and SUMO3-MCAF1-SIM complexes in their unphosphorylated forms (Sekiyama et al., 2008; Song et al., 2005). Indeed, no specific contacts were observed between the SUMO proteins and the cluster of serine/acidic residues adjacent to either the PIAS2 or MCAF1 SIM sequences (Sekiyama et al., 2008; Song et al., 2005). In contrast, the interaction module of the PML-SIM-PO_4 peptide was extended, due to the presence of the phosphorylated serine residues, and could be perceived as two distinct submodules, one corresponding to the hydrophobic residues and one encompassing the first three phosphorylated residues ($S560_{PO4}$-$S561_{PO4}$-$S562_{PO4}$) immediately adjacent to the hydrophobic residues. Thus, the extended interaction interface seen in the SUMO1:PML-SIM-PO_4 complex required the phosphorylated serine residues. More specifically, the SUMO1:PML-SIM-PO_4 structure revealed that $S560_{PO4}$, $S561_{PO4}$, and $S562_{PO4}$ generated three additional interactions with three distinct residues of SUMO1, respectively K46, K39, and H43. Interestingly, phosphorylation of the fourth serine residue (S565) in the PML serine/acidic residue cluster did not appear to make a specific interaction with SUMO1 in the crystal structure, since no corresponding density could be observed in the electron density maps. This suggests that $S565_{PO4}$ was not directly contributing to the binding of the PML phosphoSIM to SUMO1, but rather was required for the subsequent phosphorylation of S562 (Scaglioni et al., 2006), which did contribute directly to the binding to SUMO1 through an interaction with H43.

Interestingly, a number of proteins known to reside and/or transiently interact with the PML-NBs also contain phosphoSIM modules similar to the one in PML, and evidence suggests that the homeostasis of the PML-NBs is governed by SUMO-dependent noncovalent binding that is regulated in part by phosphorylation events (Lin et al., 2006; Rabellino et al., 2012; Scaglioni et al., 2006; Stehmeier and Muller, 2009). Comparing our crystal structures of the SUMO1:PML-SIM-PO_4 and SUMO1:mDaxx-SIM-PO_4 complexes indicated that there were similarities as well as intriguing differences between the two phosphoSIMs. Like the PML-SIM-PO_4 peptide, the mDaxx-SIM-PO4 peptide bound to SUMO1 in a more extended form that could be viewed as two submodules, with both the hydrophobic and phosphorylated regions of the phosphoSIM making important contributions to the binding interface. As expected, the hydrophobic regions of the SIM and the phosphorylated SIM bound in very similar manners, which was consistent with what has been observed in the structures of several other SIMs bound to SUMO proteins. However, the interactions involving the phosphorylated regions were slightly more complex.

In the case of Daxx, the phosphoSIM contained two phosphorylated serine residues ($S737_{PO4}$ and $S739_{PO4}$) separated by an aspartic acid (D738) in the first three positions immediately adjacent to the hydrophobic residues, as opposed to three phosphoserines ($S560_{PO4}$, $S561_{PO4}$, and $S562_{PO4}$) located in the same positions in the phosphoSIM of PML (Chang et al., 2011; Scaglioni et al., 2006). This aspartic acid between the two phosphoserines alters the interaction of the first two positions following the hydrophobic residues with SUMO1 with respect to what was observed with the three phosphoserines of PML. Whereas a direct contact was seen between the phosphate group of $S560_{PO4}$ from PML and K46 of SUMO1, the phosphate from $S737_{PO4}$ of Daxx was not in position to make the same interaction. The negatively charged phosphate of $S561_{PO4}$ from PML made direct contact with the positive charge of K39 from SUMO1, whereas D738 from Daxx was at hydrogen bond distance from the hydroxyl group of T42 of SUMO1 and a water molecule. Thus, a simple substitution of an aspartic acid for a phosphoserine in the second position after the hydrophobic region changed the interaction pattern in the first two positions of the phosphomodule with SUMO1. Based on these results, it appeared that the precise arrangement of phosphoserines, phosphothreonines, aspartic acids, and glutamic acids in the positions immediately after the hydrophobic regions can have a significant impact on the interactions with positively charged residues on the SUMO proteins.

It has been suggested that one potential function of the acidic and/or phosphorylated residues within the phosphoSIMs is to define binding specificity for distinct SUMO family proteins (Chang et al., 2011; Hecker et al., 2006). In support of this idea, a recent study described an interconnection between phosphoSIMs and acetylation of SUMO proteins that led to a higher-order level of selectivity (Ullmann et al., 2012). Based on the differences we observed in the crystal structures of the SUMO1:PML-SIM-PO_4 and SUMO1:mDaxx-SIM-PO_4 complexes, it appears that different arrangements of negatively charged (D and E) and phosphorylated (S and T) residues within the phosphoSIM could help define this specificity for different SUMO proteins depending on their respective phosphorylation (Figure S1B) and acetylation states. SUMO1 can be acetylated at several lysines (K37, K39, K45, K46, and K48) (Cheema et al., 2010; Choudhary et al., 2009; Ullmann et al., 2012), and three of these lysines (K37, K39, and K46) made contacts with the phosphoSIM of PML in the SUMO1-PML-SIM-PO_4 complex. More precisely, the positive charges of K46 and K39 made contact with the phosphate groups of $S560_{PO4}$ and $S562_{PO4}$, respectively, whereas the aliphatic portion of the side chain of K37 made van der Waals contact with V558 from the phosphoSIM of PML. In the case of the SUMO1-mDaxx-SIM-PO_4 complex, the van der Waals contact between K37 of SUMO1 and V735 of Daxx was very similar to what was observed between K37 and V558 of PML. However, no direct contacts were observed between the phosphoSIM of Daxx and either K39 or K46 of SUMO1. This suggests that acetylation of either of these two lysine residues could have different impact on SUMO1 binding to PML versus Daxx.

Interestingly, these results also explain how acidic and/or phosphorylatable residues at the third position of the hydrophobic core could also contribute to the specificity for SUMO proteins. In the NMR structures of the SUMO1:PIAS2-SIM and SUMO3-MCAF1-SIM complexes (Sekiyama et al., 2008; Song et al., 2005), the negative charge of an aspartic acid residue at the third position of the hydrophobic core within the SIM interacted with the positive charge of K37 or K33 of SUMO1 and SUMO2, respectively. This is in contrast to the van der Waals interaction that was observed with valine residues in the same position of the phosphoSIMs of PML and Daxx. Taken together, our structures of the SUMO1:PML-SIM-PO_4 and SUMO1:mDaxx-SIM-PO_4 complexes in

combination with previous biochemical and structural studies provide atomic level insights into how phosphorylated residues in phosphoSIMs from various proteins in PML-NBs contribute to binding to SUMO proteins. In addition, the results indicate how different spacing patterns of acidic/phosphorylated residues within both modules of the phosphoSIM, hydrophobic and phosphorylated (Figure S1B), can interconnect with the acetylation patterns of the different SUMO family proteins to control specific interactions. Biologically, this can be particularly relevant to the diverse functions attributed to PML-NBs, as exemplified by the different growth rate reductions that U2OS cells experienced (Figure 6) when comparing wild-type PML-IV with the phosphoSIM mutants.

EXPERIMENTAL PROCEDURES

Expression Vectors

BRET Constructs

The PML BRET constructs have been described previously (Percherancier et al., 2009). The nonconjugable version of human SUMO1 fused to pGFP10 was generated by site-directed mutagenesis from pGFP10-SUMO1, mutating the SUMO diglycine motif to alanine residues (Mascle et al., 2007). All SUMO1 mutants were generated by site-directed mutagenesis starting from the nonconjugable form of SUMO1.

Recombinant Protein Constructs

The sequences for the PML-SIM peptides (residues 547–573; PML-I) were ordered as oligonucleotides (Integrated DNA Technologies) and cloned as a BamHI-EcoRI fragment into pGEX-2T vector (Amersham). SUMO1 (residues 2–97 of human SUMO1) cDNA was PCR amplified from pGFP10-SUMO1 and cloned as an XbaI fragment into pGEX-4T3 vector (Amersham). A SUMO1-C52A point mutant was generated using site-directed mutagenesis. A ΔN-SUMO1 construct (residues 17–97 with the C52A mutation) was cloned into a modified pGEX-2T vector with a tobacco etch virus protease cut. Constructs were verified by DNA sequencing.

Retroviral Expression Vectors

The retroviral vectors pLPC and pLPC-PML-IV have been described previously (Ferbeyre et al., 2000). Mutations of either the hydrophobic (556-AAAS-559) or four serine (S560A, S561A, S562A, and S565A) residues were obtained by site-directed mutagenesis of pLPC-PML-IV.

BRET Experiments

The BRET assays were conducted as described previously (Percherancier et al., 2009). For details, see Supplemental Experimental Procedures.

Expression and Purification of Proteins

SUMO1, ΔN-SUMO1, and PML-SIM were expressed as GST fusion proteins in *E. coli* host strain TOPP2 (Stratagene) and purified. For details of purification, see Supplemental Experimental Procedures.

In Vitro Phosphorylation and Purification

The tetraphosphorylated PML-SIM-PO_4 peptide was generated from the PML-SIM peptide by incubation with CK2 (New England Biolabs). See Supplemental Experimental Procedures for details.

Peptide Synthesis

The mDaxx-SIM (GSGEAEERIIVLpSDpSDY) and mDaxx-SIM-PO_4 (GSGEAEERIIVLSDSDY) peptides were chemically synthesized using Fmoc chemistry. See Supplemental Experimental Procedures for details.

ITC Experiments

Proteins were dialysed overnight against buffer (20 mM Tris-HCl, pH 7.4). ITC measurements were performed at 25°C using a VP-ITC calorimeter (GE Healthcare). All titration experiments were done in duplicate and fit to a single binding site interaction with 1:1 stoichiometry. The baseline-corrected data were fit with Origin 7 software. See Supplemental Experimental Procedures for details.

NMR Spectroscopy

NMR chemical shift perturbation experiments were carried out at 300K on either a Varian Unity Inova 500 or 600 MHz spectrometer. For details, see Supplemental Experimental Procedures.

Crystallization and Data Collection

Crystals of each complex were obtained by the hanging drop vapor diffusion method and data were collected at the Canadian Light Source (CLS) or National Synchrotron Light Source (NSLS). See Supplemental Experimental Procedures for details.

Structure Determination and Refinement

Initial phases were obtained by molecular replacement using the crystal structure of ΔN-SUMO1 (Protein Data Bank [PDB] ID 2UYZ) as a search template. Phases were improved by iterative cycles of model building with Coot and refinement with Phenix. Test data sets were randomly selected from the observed reflections prior to refinement. The figures were prepared with PyMOL.

Cell Proliferation, Immunoblotting, and Immunofluorescence

Cell proliferation assays in U2OS cells (Ferbeyre et al., 2000), immunoblots (Ferbeyre et al., 2000), and immunofluorescence experiments (Vernier et al., 2011) were performed as described previously. See Supplemental Experimental Procedures for details on these assays.

ACCESSION NUMBERS

The PDB accession numbers for the structures reported in this paper are 4WJN, 4WJO, 4WJP, and 4WJQ.

SUPPLEMENTAL INFORMATION

Supplemental Information includes Supplemental Experimental Procedures, four figures, and four 3D molecular models and can be found with this article online at http://dx.doi.org/10.1016/j.str.2014.10.015.

AUTHOR CONTRIBUTIONS

L.C., X.M., V.B., S.T.-B., M.C.-M., M.L.-P., and J.W. prepared reagents and conducted experiments. L.C., X.M., V.B., M.L.-P., K.S., M.A., G.F., and J.G.O. designed experiments and wrote the manuscript.

ACKNOWLEDGMENTS

We thank Mounira Chelbi-Alix for the PML-4SA and PML-4SD constructs used in the BRET studies. This work was supported by grants from the Canadian Institutes for Health Research (to J.G.O., 74739 and 130414, and G.F., 130562) as well as from the Natural Sciences and Engineering Research Council of Canada (to M.A.). L.C. is a postdoctoral fellow of the Natural Sciences and Engineering Research Council of Canada CREATE program. Research described in this work was carried out in part at the National Synchrotron Light Source, Brookhaven National Laboratory, which is supported by the United States Department of Energy, Division of Materials Sciences and Division of Chemical Sciences under contract DE-AC02-98CH10886, and at the Canadian Light Source, which is supported by the Natural Sciences and Engineering Research Council of Canada, the National Research Council Canada, the Canadian Institutes of Health Research, the Province of Saskatchewan, Western Economic Diversification Canada, and the University of Saskatchewan.

Received: August 11, 2014
Revised: October 7, 2014
Accepted: October 13, 2014
Published: December 11, 2014

REFERENCES

Armstrong, A.A., Mohideen, F., and Lima, C.D. (2012). Recognition of SUMO-modified PCNA requires tandem receptor motifs in Srs2. Nature *483*, 59–63.

Bischof, O., Kirsh, O., Pearson, M., Itahana, K., Pelicci, P.G., and Dejean, A. (2002). Deconstructing PML-induced premature senescence. EMBO J. *21*, 3358–3369.

Chang, C.-C., Naik, M.T., Huang, Y.-S., Jeng, J.-C., Liao, P.-H., Kuo, H.-Y., Ho, C.-C., Hsieh, Y.-L., Lin, C.-H., Huang, N.-J., et al. (2011). Structural and functional roles of Daxx SIM phosphorylation in SUMO paralog-selective binding and apoptosis modulation. Mol. Cell *42*, 62–74.

Cheema, A., Knights, C.D., Rao, M., Catania, J., Perez, R., Simons, B., Dakshanamurthy, S., Kolukula, V.K., Tilli, M., Furth, P.A., et al. (2010). Functional mimicry of the acetylated C-terminal tail of p53 by a SUMO-1 acetylated domain, SAD. J. Cell. Physiol. *225*, 371–384.

Chen, Y.-C.M., Kappel, C., Beaudouin, J., Eils, R., and Spector, D.L. (2008). Live cell dynamics of promyelocytic leukemia nuclear bodies upon entry into and exit from mitosis. Mol. Biol. Cell *19*, 3147–3162.

Cho, G., Lim, Y., and Golden, J.A. (2009). SUMO interaction motifs in Sizn1 are required for promyelocytic leukemia protein nuclear body localization and for transcriptional activation. J. Biol. Chem. *284*, 19592–19600.

Choudhary, C., Kumar, C., Gnad, F., Nielsen, M.L., Rehman, M., Walther, T.C., Olsen, J.V., and Mann, M. (2009). Lysine acetylation targets protein complexes and co-regulates major cellular functions. Science *325*, 834–840.

Danielsen, J.R., Povlsen, L.K., Villumsen, B.H., Streicher, W., Nilsson, J., Wikström, M., Bekker-Jensen, S., and Mailand, N. (2012). DNA damage-inducible SUMOylation of HERC2 promotes RNF8 binding via a novel SUMO-binding Zinc finger. J. Cell Biol. *197*, 179–187.

Dellaire, G., and Bazett-Jones, D.P. (2007). Beyond repair foci: subnuclear domains and the cellular response to DNA damage. Cell Cycle *6*, 1864–1872.

Dellaire, G., Ching, R.W., Ahmed, K., Jalali, F., Tse, K.C.K., Bristow, R.G., and Bazett-Jones, D.P. (2006). Promyelocytic leukemia nuclear bodies behave as DNA damage sensors whose response to DNA double-strand breaks is regulated by NBS1 and the kinases ATM, Chk2, and ATR. J. Cell Biol. *175*, 55–66.

Desterro, J.M.P., Rodriguez, M.S., Kemp, G.D., and Hay, R.T. (1999). Identification of the enzyme required for activation of the small ubiquitin-like protein SUMO-1. J. Biol. Chem. *274*, 10618–10624.

Everett, R.D., Lomonte, P., Sternsdorf, T., van Driel, R., and Orr, A. (1999). Cell cycle regulation of PML modification and ND10 composition. J. Cell Sci. *112*, 4581–4588.

Ferbeyre, G., de Stanchina, E., Querido, E., Baptiste, N., Prives, C., and Lowe, S.W. (2000). PML is induced by oncogenic ras and promotes premature senescence. Genes Dev. *14*, 2015–2027.

Gareau, J.R., and Lima, C.D. (2010). The SUMO pathway: emerging mechanisms that shape specificity, conjugation and recognition. Nat. Rev. Mol. Cell Biol. *11*, 861–871.

Gareau, J.R., Reverter, D., and Lima, C.D. (2012). Determinants of small ubiquitin-like modifier 1 (SUMO1) protein specificity, E3 ligase, and SUMO-RanGAP1 binding activities of nucleoporin RanBP2. J. Biol. Chem. *287*, 4740–4751.

Hecker, C.M., Rabiller, M., Haglund, K., Bayer, P., and Dikic, I. (2006). Specification of SUMO1- and SUMO2-interacting motifs. J. Biol. Chem. *281*, 16117–16127.

Husnjak, K., and Dikic, I. (2012). Ubiquitin-binding proteins: decoders of ubiquitin-mediated cellular functions. Annu. Rev. Biochem. *81*, 291–322.

Ishov, A.M., Sotnikov, A.G., Negorev, D., Vladimirova, O.V., Neff, N., Kamitani, T., Yeh, E.T.H., Strauss, J.F., 3rd, and Maul, G.G. (1999). PML is critical for ND10 formation and recruits the PML-interacting protein daxx to this nuclear structure when modified by SUMO-1. J. Cell Biol. *147*, 221–234.

Jensen, K., Shiels, C., and Freemont, P.S. (2001). PML protein isoforms and the RBCC/TRIM motif. Oncogene *20*, 7223–7233.

Kahyo, T., Nishida, T., and Yasuda, H. (2001). Involvement of PIAS1 in the sumoylation of tumor suppressor p53. Mol. Cell *8*, 713–718.

Lallemand-Breitenbach, V., and de Thé, H. (2010). PML nuclear bodies. Cold Spring Harb. Perspect. Biol. *2*, a000661.

Lin, D.-Y., Huang, Y.-S., Jeng, J.-C., Kuo, H.-Y., Chang, C.-C., Chao, T.-T., Ho, C.-C., Chen, Y.-C., Lin, T.-P., Fang, H.-I., et al. (2006). Role of SUMO-interacting motif in Daxx SUMO modification, subnuclear localization, and repression of sumoylated transcription factors. Mol. Cell *24*, 341–354.

Maroui, M.A., Kheddache-Atmane, S., El Asmi, F., Dianoux, L., Aubry, M., and Chelbi-Alix, M.K. (2012). Requirement of PML SUMO interacting motif for RNF4- or arsenic trioxide-induced degradation of nuclear PML isoforms. PLoS ONE *7*, e44949.

Mascle, X.H., Germain-Desprez, D., Huynh, P., Estephan, P., and Aubry, M. (2007). Sumoylation of the transcriptional intermediary factor 1beta (TIF1beta), the Co-repressor of the KRAB Multifinger proteins, is required for its transcriptional activity and is modulated by the KRAB domain. J. Biol. Chem. *282*, 10190–10202.

Negorev, D., Ishov, A.M., and Maul, G.G. (2001). Evidence for separate ND10-binding and homo-oligomerization domains of Sp100. J. Cell Sci. *114*, 59–68.

Olsen, S.K., Capili, A.D., Lu, X., Tan, D.S., and Lima, C.D. (2010). Active site remodelling accompanies thioester bond formation in the SUMO E1. Nature *463*, 906–912.

Percherancier, Y., Germain-Desprez, D., Galisson, F., Mascle, X.H., Dianoux, L., Estephan, P., Chelbi-Alix, M.K., and Aubry, M. (2009). Role of SUMO in RNF4-mediated promyelocytic leukemia protein (PML) degradation: sumoylation of PML and phospho-switch control of its SUMO binding domain dissected in living cells. J. Biol. Chem. *284*, 16595–16608.

Pichler, A., Gast, A., Seeler, J.S., Dejean, A., and Melchior, F. (2002). The nucleoporin RanBP2 has SUMO1 E3 ligase activity. Cell *108*, 109–120.

Rabellino, A., Carter, B., Konstantinidou, G., Wu, S.-Y., Rimessi, A., Byers, L.A., Heymach, J.V., Girard, L., Chiang, C.-M., Teruya-Feldstein, J., and Scaglioni, P.P. (2012). The SUMO E3-ligase PIAS1 regulates the tumor suppressor PML and its oncogenic counterpart PML-RARA. Cancer Res. *72*, 2275–2284.

Rasheed, Z.A., Saleem, A., Ravee, Y., Pandolfi, P.P., and Rubin, E.H. (2002). The topoisomerase I-binding RING protein, topors, is associated with promyelocytic leukemia nuclear bodies. Exp. Cell Res. *277*, 152–160.

Reverter, D., and Lima, C.D. (2005). Insights into E3 ligase activity revealed by a SUMO-RanGAP1-Ubc9-Nup358 complex. Nature *435*, 687–692.

Salomoni, P., Bernardi, R., Bergmann, S., Changou, A., Tuttle, S., and Pandolfi, P.P. (2005). The promyelocytic leukemia protein PML regulates c-Jun function in response to DNA damage. Blood *105*, 3686–3690.

Salomoni, P., Dvorkina, M., and Michod, D. (2012). Role of the promyelocytic leukaemia protein in cell death regulation. Cell Death Dis. *3*, e247.

Scaglioni, P.P., Yung, T.M., Cai, L.F., Erdjument-Bromage, H., Kaufman, A.J., Singh, B., Teruya-Feldstein, J., Tempst, P., and Pandolfi, P.P. (2006). A CK2-dependent mechanism for degradation of the PML tumor suppressor. Cell *126*, 269–283.

Scaglioni, P.P., Yung, T.M., Choi, S., Baldini, C., Konstantinidou, G., and Pandolfi, P.P. (2008). CK2 mediates phosphorylation and ubiquitin-mediated degradation of the PML tumor suppressor. Mol. Cell. Biochem. *316*, 149–154.

Sekiyama, N., Ikegami, T., Yamane, T., Ikeguchi, M., Uchimura, Y., Baba, D., Ariyoshi, M., Tochio, H., Saitoh, H., and Shirakawa, M. (2008). Structure of the small ubiquitin-like modifier (SUMO)-interacting motif of MBD1-containing chromatin-associated factor 1 bound to SUMO-3. J. Biol. Chem. *283*, 35966–35975.

Shen, L.N., Dong, C., Liu, H., Naismith, J.H., and Hay, R.T. (2006). The structure of SENP1-SUMO-2 complex suggests a structural basis for discrimination between SUMO paralogues during processing. Biochem. J. *397*, 279–288.

Song, J., Durrin, L.K., Wilkinson, T.A., Krontiris, T.G., and Chen, Y. (2004). Identification of a SUMO-binding motif that recognizes SUMO-modified proteins. Proc. Natl. Acad. Sci. USA *101*, 14373–14378.

Song, J., Zhang, Z., Hu, W., and Chen, Y. (2005). Small ubiquitin-like modifier (SUMO) recognition of a SUMO binding motif: a reversal of the bound orientation. J. Biol. Chem. *280*, 40122–40129.

Stehmeier, P., and Muller, S. (2009). Phospho-regulated SUMO interaction modules connect the SUMO system to CK2 signaling. Mol. Cell *33*, 400–409.

Sung, K.S., Lee, Y.-A., Kim, E.T., Lee, S.-R., Ahn, J.-H., and Choi, C.Y. (2011). Role of the SUMO-interacting motif in HIPK2 targeting to the PML nuclear bodies and regulation of p53. Exp. Cell Res. *317*, 1060–1070.

Ullmann, R., Chien, C.D., Avantaggiati, M.L., and Muller, S. (2012). An acetylation switch regulates SUMO-dependent protein interaction networks. Mol. Cell *46*, 759–770.

Vernier, M., Bourdeau, V., Gaumont-Leclerc, M.-F., Moiseeva, O., Bégin, V., Saad, F., Mes-Masson, A.-M., and Ferbeyre, G. (2011). Regulation of E2Fs and senescence by PML nuclear bodies. Genes Dev. *25*, 41–50.

Weidtkamp-Peters, S., Lenser, T., Negorev, D., Gerstner, N., Hofmann, T.G., Schwanitz, G., Hoischen, C., Maul, G., Dittrich, P., and Hemmerich, P. (2008). Dynamics of component exchange at PML nuclear bodies. J. Cell Sci. *121*, 2731–2743.

Zhong, S., Salomoni, P., and Pandolfi, P.P. (2000). The transcriptional role of PML and the nuclear body. Nat. Cell Biol. *2*, E85–E90.

